Deformation-induced delamination of photovoltaic modules by foaming ethylene-vinyl acetate with supercritical CO2

Axel Briand, Antoine Leybros, Olivier Doucet, Marion Vite, Ayoub Gasmi, Jean Christophe Ruiz, Fabrice Lamadie, Agnès Grandjean

Deformation-induced delamination of photovoltaic modules by foaming ethylene-vinyl acetate with supercritical CO_2

*Axel Briand[1,2], *Antoine Leybros[1], Olivier Doucet[2], Marion Vite[2], Ayoub Gasmi[2], Jean Christophe Ruiz[1], Fabrice Lamadie[1], Agnès Grandjean[1]

1- CEA, DES, ISEC, DMRC, Univ Montpellier, Marcoule, France

2- Univ Grenoble Alpes, CEA, DRT, LITEN, DTS, INES, F-38 000 Grenoble, France.

*Corresponding authors:

Axel BRIAND
CEA
Laboratoire des Procédés Supercritiques et de Décontamination
F-30207 Bagnols sur Cèze
Tel: +33 4 66 79 18 93
Fax: +33 4 66 79 18 93
axel.briand@cea.fr

Antoine LEYBROS
CEA
Laboratoire des Procédés Supercritiques et de Décontamination
F-30207 Bagnols sur Cèze
Tel: +33 4 66 79 16 41
Fax: +33 4 66 79 16 41
antoine.leybros@cea.fr

Abstract

Photovoltaic panels are an important source of renewable energy but also represent a growing stock of complex electronic waste. Specific recycling processes are required and this article investigates the potential of supercritical CO_2 foaming of the ethylene-vinyl acetate (EVA) in photovoltaic modules as a means of safely taking them apart, layer by layer. The effects of the CO_2 temperature, pressure and depressurization rate on the deformation of EVA layers were characterized using in-situ measurements of area expansion and curvature during the foaming process. Peel tests were performed on treated and untreated samples to quantify the loss of adhesion at the different EVA interfaces. The data show that with the temperature

set above the melting point and an initial pressure of at least 150 bar, the deformation of the EVA layers can be increased by increasing the depressurization rate. The correlation between the percentage loss of adhesion and area expansion of the EVA layers shows that the mechanical stress induced by deformation is an important factor in the delamination process; however, the amount of separation achieved and the optimal combination operating parameters depend on the nature and morphology of the neighbouring layer (glass, cell frontside or backsheet). These results are an important first step in the development of an efficient recycling process for photovoltaic modules and other types of layered electronic devices.

Keywords: supercritical CO_2, photovoltaic, recycling, polymer, foaming, expansion.

1. Introduction

The number of end-of-life (EOL) photovoltaic (PV) panels to be disposed of or recycled will increase substantially over the next decade [1]. A crystalline silicon-based PV panel consists of a PV module stiffened by an aluminum frame and electrically controlled by a junction box. The PV module itself is a set of electrically connected crystalline silicon cells sandwiched between two layers of encapsulating polymer, a glass front face and a polymer "backsheet" (**Fig. 1**). The encapsulating polymer used in more than 90% of PV panels as of 2019 was , ethylene-vinyl acetate (EVA) [2]. The EVA inside PV modules is a semi-crystalline elastomer. The "backsheet" is a multilayer assembly of polymers, most often a polyethylene terephthalate (PET) core layer sandwiched between two layers. The outer layer is generally made of a fluoropolymer such as poly(vinylidene fluoride) (PVDF).

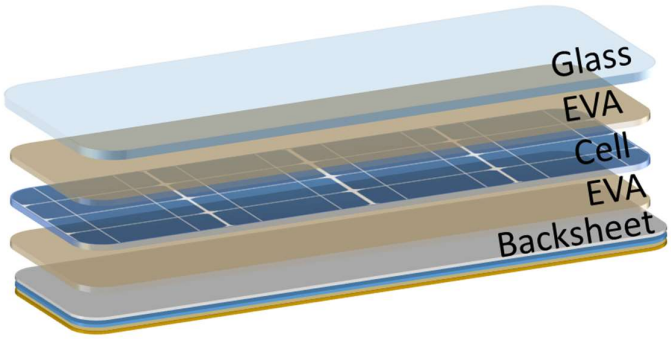

Fig. 1. Schematic representation of the different layers in a photovoltaic module.

Efficient recycling processes are essential to satisfy the growth in energy demand while transitioning to a greener circular economy. Existing chemical [3,4], mechanical [5]. and thermal [6] treatment processes are poorly selective and produce environmentally harmful gaseous or liquid effluents [7]. Delamination using supercritical CO_2 (SC-CO_2) is attractive in this context as a greener means of recycling EOL PV modules. Indeed, PV module delamination by the use of organic solvents coupled to SC-CO_2 to reduce the treatment time and to reduce the liquid effluent volume is described in the literature [8,9]. Unlike the latter, a delamination process using only SC-CO_2 is presented in this document. The main benefits of this process are that the module is separated layer by layer without breaking the glass, contaminating any of the valuable materials (silver, silicon and glass), or producing any liquid effluents. The delamination mechanism is illustrated in **Fig. 2.** the polymer absorbs SC-CO_2 [10] before rapid depressurization (> 0.5 bar$\cdot$s^{-1}) leads to foaming, which as observed for various polymers [11–14], can lead to loss of adhesion at the interfaces [15] and separation [16].

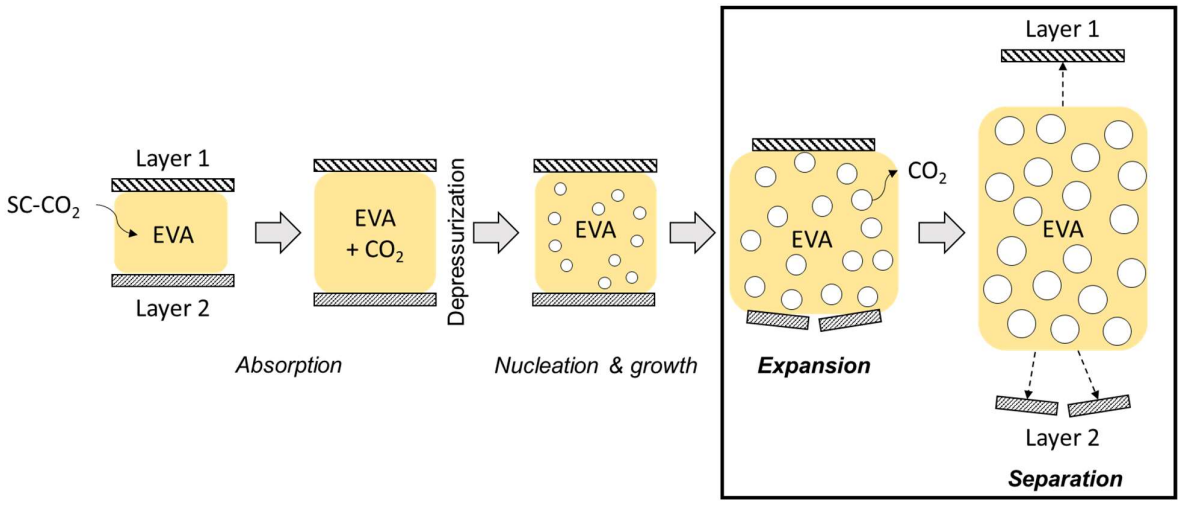

Fig. 2. Schematic diagram of the different stages through which delamination is achieved by foaming a polymer (in this case ethylene-vynil acetate, EVA) with supercritical CO_2 (SC-CO_2).

The expansion behaviour of polymers foamed with physical agents is typically studied using post-treatment measurements [13] and data from direct observations of the expansion process are rare [17,18]. It is generally recognized [13] that this depends mainly on the physical state of the polymer, with temperatures around the polymer melting point being optimal to maximize the expansion ratio [17,19]. However, while expansion studies have mainly been performed on liquid polymers used in extrusion processes [17,19–22], the polymer most commonly used in PV modules (and the one studied here), EVA, is a solid elastomer foamed by batch-processing. To our knowledge, the only existing data on EVA expansion induced by foaming with CO_2 come from Sarver et al.'s study of crosslinked EVA-25 at pressures ranging from 100 to 300 bar and temperatures of 30 to 60 °C (below the melting point) [23]. Furthermore, the effects on the foaming process of barrier interfaces, as formed by the neighbouring layers in PV modules, have only ever been studied for a metallic structure [24] and various polymer films [25]. Mechanical constraints and polymer deformation at the interfaces are likely to affect the foaming process but these effects have never been observed in-situ. The aim of this study was therefore to use direct observations of PV modules during

SC-CO_2 foaming of the polymer layers complemented by peel tests to explain the influence of pressure, temperature and the depressurization rate on the loss of adhesion at each of the interfaces.

2. Experimental

2.1. Materials

The EVA-28 used in this study (28 wt.% vinyl acetate; Guangzhou Lushan New Materials Co; Guangdong Province, China) was produced by radical polymerization and shaped into 600 µm thick films containing cross-linking agents (peroxides) for hot lamination (> 120 °C). The EVA-28 films were included in a PV module equipped with a Si-Al-BSF cell design and sandwiched with a 3 mm thick soda-lime glass front face and a primer layer/PET/PVDF backsheet. Carbon dioxide (> 99.99% purity) was procured from Air Liquide (Saint Priest, France).

2.2. In-situ observation of EVA layers deformations induced by SC-CO_2 foaming

2.2.1. High-pressure device and deformation measurements

The EVA deformations induced by SC-CO_2 foaming were measured using a camera attached to a high-pressure cell with transparent sapphire windows (**Fig. 3**). This setup has been described in detail elsewhere [10]. The CO_2 was injected using a high-pressure pump (HPP400-B, SFE process, Vandœuvre-lès-Nancy, France) equipped with a pressure regulation system and connected to a recirculating chiller (ProfilCool Exactus, National Lab GmbH, Mölln, Germany).

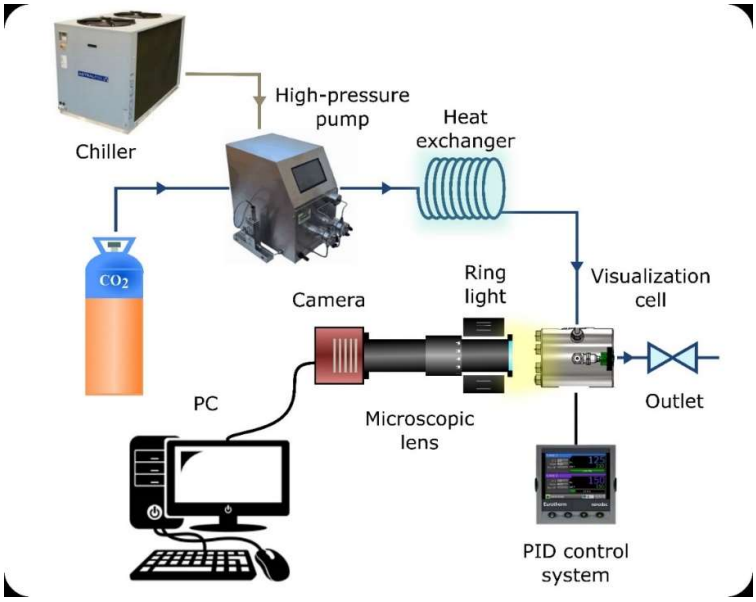

Fig. 3. Schematic diagram of the experimental setup used to observe the deformation of the ethylene-vinyl acetate layers in a photovoltaic module during foaming with supercritical CO_2.

For each foaming experiment, 2.5 cm × 1 cm PV module samples were loaded in advance into a 74 mL capacity high-pressure cell (A085FR, SFE Process, Vandœuvre-lès-Nancy, France), where they were contacted with SC-CO_2. The depressurization ramps (**Fig. 4**) were adjusted by controlling the opening diameter using a fine control valve (SS-SS2, Swagelok, Solon, United states of America). The depressurization rate was calculated linearly as the pressure difference from start (100–200 bar) to finish (atmospheric pressure) divided by the time taken to reach atmospheric pressure (**Fig. 4**). The operating parameters were varied in turn as shown in **Table 1.**

Table 1. Parameter values and parameter combinations used for the supercritical CO_2 foaming experiments

Parameter studied	Measurement error	Range	Fixed parameters
Temperature	± 0.5 °C	60–90 °C	150 bar, 1.7 bar·s^{-1}

Pressure	± 2 bar	100–200 bar	75 °C, 1.7 bar·s^{-1}
Depressurization rate	± 0.2 bar.s^{-1}	0.9–2.7 bar·s^{-1}	75 °C, 150 bar

The deformation of the EVA layer (**Fig. 5**) was measured using a frontlight setup (**Fig. 3**). The light source was a green LED ring light (Optoenginnering, 81 mm outer diameter, 60° illuminating cone), which illuminated the entire sample in a homogeneous manner. The camera (CMOS, Thorlabs; 5 megapixels, with a pixel size of 3.5 µm × 3.5 µm) was equipped with a high magnification lens (zero distortion macro lens from Optoenginnering; magnification of 9.8 µm per pixel). The acquisitions were stopped when the pressure had decreased to about 8 bar (**Fig. 4)**, which corresponded to the maximum expansion of the of EVA layers.

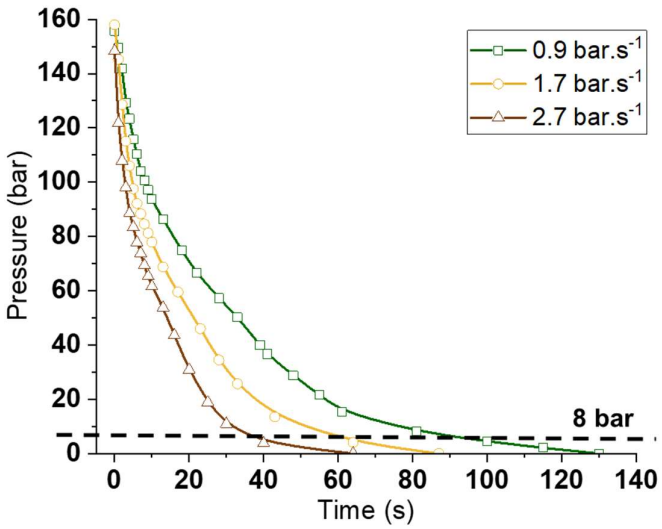

Fig. 4. Depressurization ramps with depressurization rates of 0.9, 1.7 and 2.7 bar·s^{-1}, used to study the delamination of photovoltaic modules by foaming the ethylene-vinyl acetate layers with supercritical CO_2.

2.2.2. Image processing

EVA layers, sandwiched in PV module samples, foamed by supercritical CO_2 generate deformations relatively smooth adapted to image processing (**Fig. 5**). The deformations are expansion, in both dimensions observed but mainly vertically, and curvature (**Fig. 5.d**).

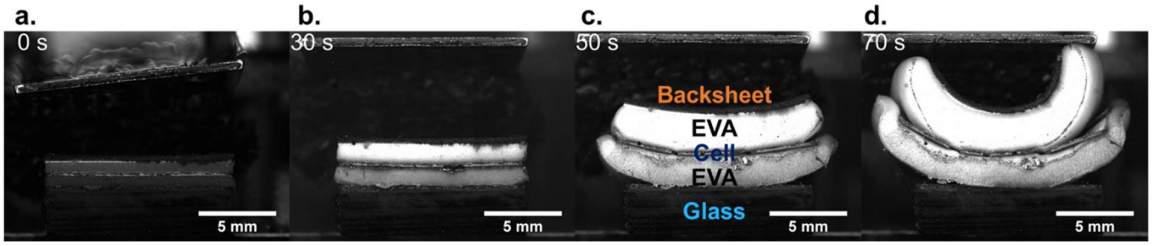

Fig. 5. Example of a sequence of images (9.8 µm/pixel) of ethylene-vinyl acetate layers in a photovoltaic module sample during foaming with supercritical CO_2 at 75 °C, 200 bar and a depressurization rate of 1.7 bar·s^{-1} after **(a)** 0 s, **(b)** 30 s, **(c)** 50 s, and **(d)** 70 s. The full video is included in the supplementary material.

The uncertainty on the imaging measurements was estimated to be 10 % based on a previous study of EVA swelling with CO_2 [10], a level of uncertainty that was confirmed by repeatability tests and is reported in the form of error bars on the graphs. The deformation of the EVA layers was characterized using a series of images recorded during the foaming process (**Fig. 5**). The raw images were processed using thanks to an image processing and the maximum Feret diameter (FD_{max}, the largest dimension) and surface area of the layers were obtained from the binarised images (**Fig. 6**). The surface area considered was the EVA layers in contact with the visualization window (**Fig. 6c**).

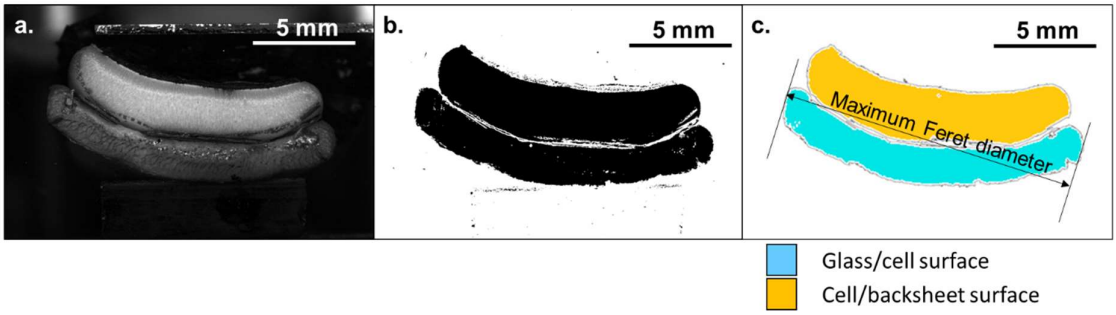

Fig. 6. (a) Raw, **(b)** binarized and **(c)** fully processed image (9.8 µm/pixel) of the ethylene-vinyl acetate (EVA) layers in a photovoltaic module during foaming with supercritical CO_2. All processing steps were performed using image processing. In part **(c)** the EVA layer between the glass and the surface of the cell is coloured in blue and the one between the cell and the backsheet is coloured in orange.

2.2.3. Final area expansion

For studying the overall mechanical stress, the final area expansion (%) was calculated as the relative increase in surface area over the entire experiment:

$$\text{Final area expansion (\%)} = \frac{S_{\text{end}} - S_{\text{start}}}{S_{\text{start}}} \times 100 \quad (1)$$

where S_{start} and S_{end} are the areas of the EVA layers measured respectively at the start and the end of the foaming experiment, as illustrated in **Fig. 6c**.

2.2.4. Longitudinal expansion

For studying the deformation linked to the shear stress; the longitudinal expansion at time *t* was similarly defined as the relative increase in the maximum Feret diameter of the layer:

$$\text{Longitudinal expansion (\%)} = \frac{FD_t - FD_{t=0}}{FD_{t=0}} \times 100 \quad (2)$$

2.2.5. Curvature

For studying the deformations linked to the mechanical constraints as tensile or peeling stresses, the curvature generated by the expansion of the EVA in contact with the other layers

was measured using an in-house image processing algorithm (**Fig. 7**). The raw images were first binarized with a threshold to only extract the projected area of the EVA layers (**Fig. 7a**). The images were then divided to separately analysing the lower and the upper EVA layer (**Fig. 7b**). Any gaps in the areas of interest due to binarization were filled in numerically and edges were smoothed by applying a morphological opening with a disc-shaped structuring element. The Cartesian coordinates of the upper and lower edges were then fitted with a parabola (**Fig. 7c**). ($Ax^2 + Bx + C$), chosen to account for the early stages of the expansion process where the profiles are almost parallel to the horizontal axis of the images and are therefore difficult to fit with a circle. The A curvature coefficient (in $pixel^{-1}$) was converted to m^{-1} using the conversion factor (9.8 µm per pixel) determined using an internal length reference (the same one for all experiments).

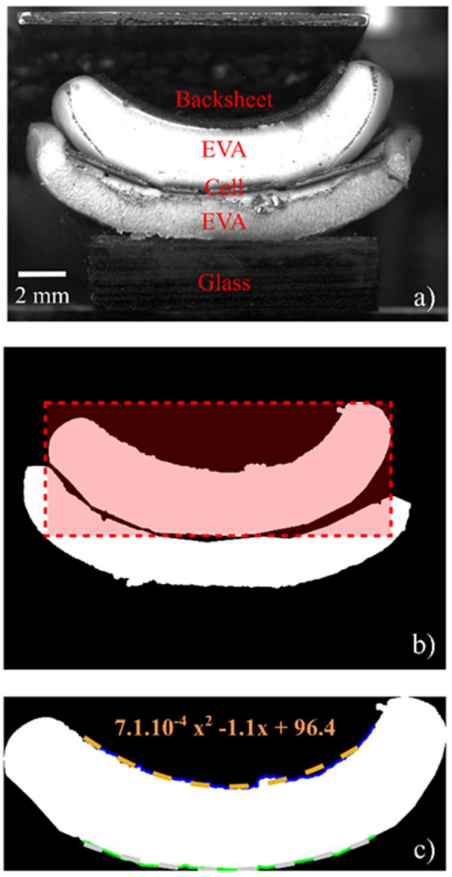

Fig. 7. Illustration of the different stages of the image processing protocol used to determine the parabolic curvature of the two edges of the ethylene-vinyl acetate (EVA) layers in photovoltaic module samples during foaming experiments with supercritical CO_2: **(a)** the raw image, **(b)** after binarization and **(c)** after selection of the EVA layer at the EVA/backsheet interface.

2.3. Adhesion measurements

Adhesion between two materials is mediated by physicochemical interactions (adsorption theory) [26–29], electrostatic interactions, mechanical interactions (mechanical adhesion theory) [30–32] and/or the interdiffusion of polymer macromolecules (diffusion

theory) [33,34]. The types of adhesion at the different EVA interfaces in a PV module are presented in **Fig. 8**.

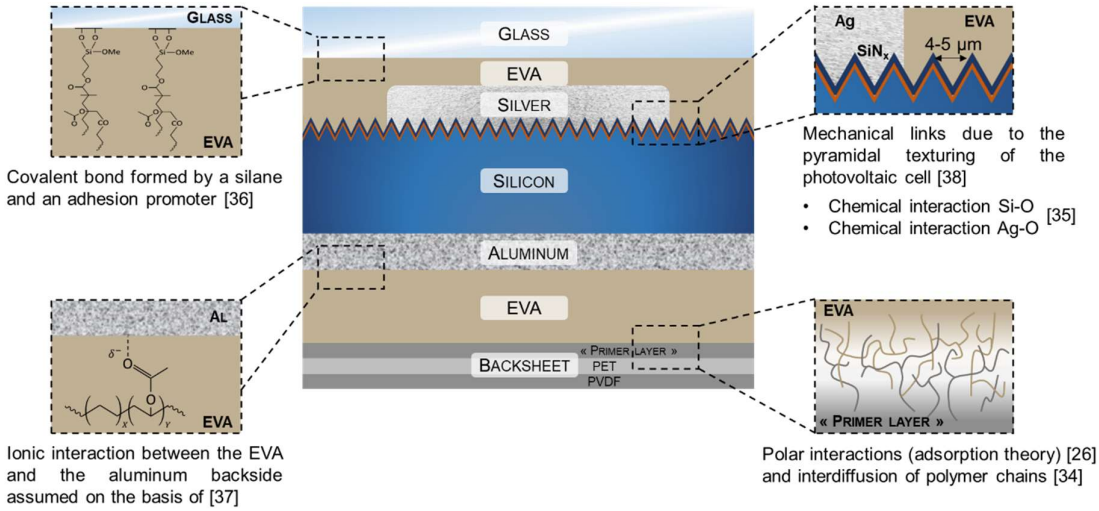

Fig. 8. Cross-sectional view of a photovoltaic module with schematic representations of the different forms of adhesion at the different interfaces of the ethylene-vinyl acetate (EVA) layer [26,34–38]

Adhesion strength (or loss of adhesion in a photovoltaic module) is typically measured experimentally by performing peel tests [39–43], which quantify the load required to separate the adherend from the substrate.

2.3.1. 180° peel tests

180° peel tests were performed using a universal testing machine (**Fig. 9a**). The applied force (in N) was converted to $N \cdot mm^{-1}$ by dividing by the width of the peel strip (10 mm). The adhesion strength of the surfaces in contact with the EVA layers (glass, front side of the cell, rear side of the cell and backsheet) in the PV module samples were measured in this way before and after treatment with SC-CO_2.

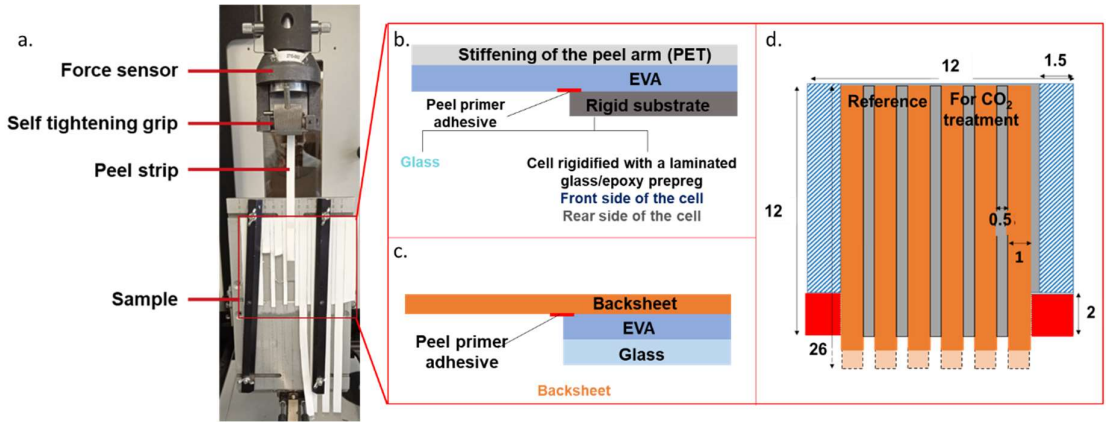

Fig. 9. (a) Photograph of the universal testing machine set up to perform 180° peel test with a photovoltaic module sample. **(b)** Cross-sectional diagram of the layer structure of the glass, cell frontside and cell backside samples**. (c)** Cross-sectional diagram of the layer structure of the backsheet samples. **(d)** Top view of a series of 180° peel test samples (with dimensions in cm).

The samples for the peel tests were prepared using a specific protocol to allow each of the interfaces to be studied separately (**Fig. 9b–d**). The interfaces of the cell were stiffened using a glass fiber/epoxy prepreg and an adhesive strip was added to initiate peeling. The peel arm was a layer of backsheet for the backsheet interface and a layer of PET for the other interfaces (**Fig. 9b,c**) The samples were 12 cm × 12 cm in size (suitable for the SC-CO_2 autoclave) and consisted of six 10 mm wide specimens: three reference specimens peeled before the SC-CO_2 treatment and three specimens peeled after treatment (**Fig. 9d**), to compare the adhesion strength of the layers before and after treatment (**Fig. 10**).

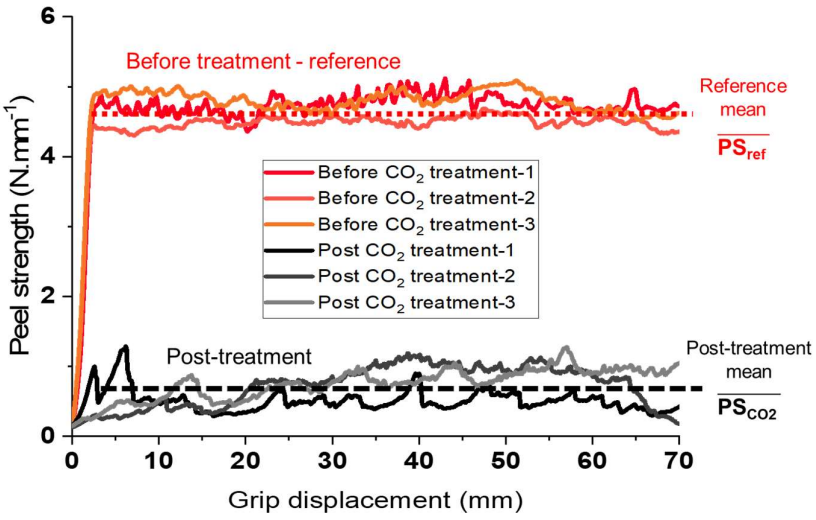

Fig. 10. Example of 180° peel test rests: peel strength as function of grip displacement for the backsheet/EVA interface before and after SC- CO_2 treatment

The relative loss of adhesion after supercritical CO_2 treatment was calculated as follows:

$$\text{Loss of adhesion (\%)} = \frac{\overline{PS_{REF}} - \overline{PS_{CO2}}}{\overline{PS_{REF}}} \times 100 \quad (3)$$

where $\overline{PS_{REF}}$ is the reference peel strength (in red in **Fig. 10**) measured before CO_2 treatment and $\overline{PS_{CO2}}$ is the peel strength (in black in **Fig. 10**) measured after CO_2 treatment. The reference peel strengths of the glass, cell frontside, cell backside, and backsheet interfaces with EVA were respectively 12.8 ± 0.7, 6.6 ± 0.3, 0.8 ± 0.2, and 4.6 ± 0.6 $N \cdot mm^{-1}$. The uncertainty of the measurements was estimated by the standard deviation of measurements performed on three identical specimens for all samples (~21 references specimens by interface).

2.3.2. Supercritical CO_2 treatment protocol

After peeling the three reference specimens in each of the four samples (one per interface studied), these were placed in a 12 L autoclave connected to a complete SC-CO_2 pilot assembly providing semi-automatic control of the experiments. The samples were contacted

with SC-CO_2 for 6 h before depressurization, about three times longer than the thermal equilibration time of CO_2/EVA (about 2 h) [10]. The free volume in the autoclave was filled with cylinders made of high-density polyethylene (a material not sensitive to CO_2 for the operating parameters used here) to increase the depressurization rate. The cylinders were 5 cm high and of a suitable diameter to fill the autoclave. The fastest depressurization rate achievable with this setup was 2.7 bar·s^{-1}.

The results for the EVA interface with the rear side of the cell are not studied here because the peel force was found to be much lower than that of the other interfaces (about 1 N·mm^{-1}), and after SC-CO_2 treatment, the peeling occurred inside the aluminium layer rather than at the interface (**Fig. 11**).

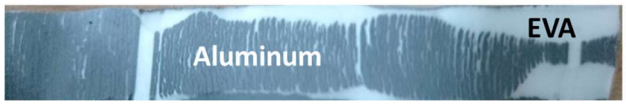

Fig. 11. Photograph of a peeled specimen of the EVA interface with the rear side of the cell, with aluminium visible on its surface**.**

3. Results and discussion

3.1. Effect of CO_2 pressure, temperature and depressurization rate on EVA layer deformation

3.1.1. Effect of the CO_2 depressurization rate on EVA expansion

Fig. 12 shows similar trends in the area expansion (**Fig. 12a**), longitudinal expansion (**Fig. 12b**) and curvature (**Fig. 12c**) of the EVA layers, with no change observed during the nucleation phase and a sharp increase once the pressure drops to ~35 bar and the EVA begins to expand. The longitudinal expansion and curvature rates were determined for each sample from linear fits of the data in the expansion phase.

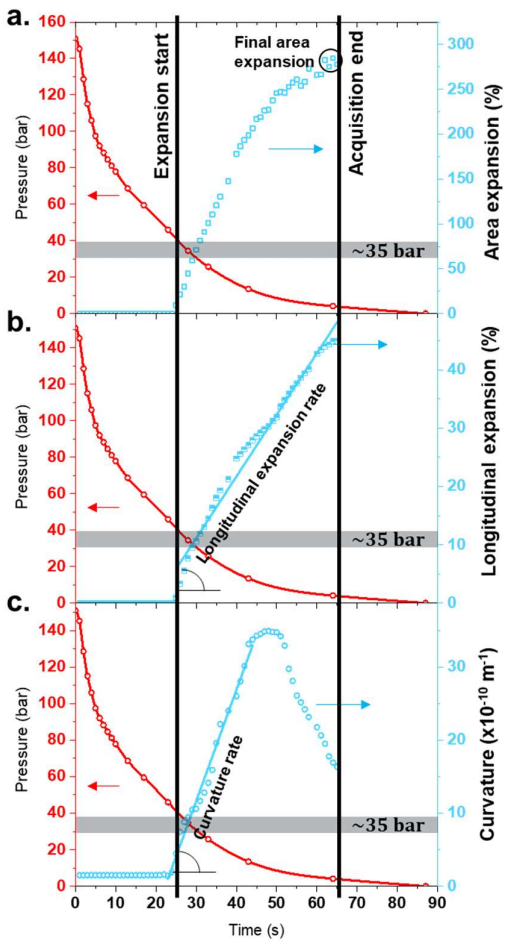

Fig. 12. (a) Area expansion (Eq. 1), **(b)** longitudinal expansion (Eq. 2) and **(c)** curvature of the ethylene-vinyl acetate (EVA) layer at the EVA/glass interface of a photovoltaic module in supercritical CO_2 during depressurization at 1.7 bar·s^{-1} from 150 bar, 75 °C.

Fig. 13 shows that the maximum area expansion, the longitudinal expansion rate and the curvature rate of both EVA layers increase gradually with the depressurization rate. Increasing this operating parameter increases the mechanical stress at the different interfaces induced by EVA foaming and should therefore facilitate delamination.

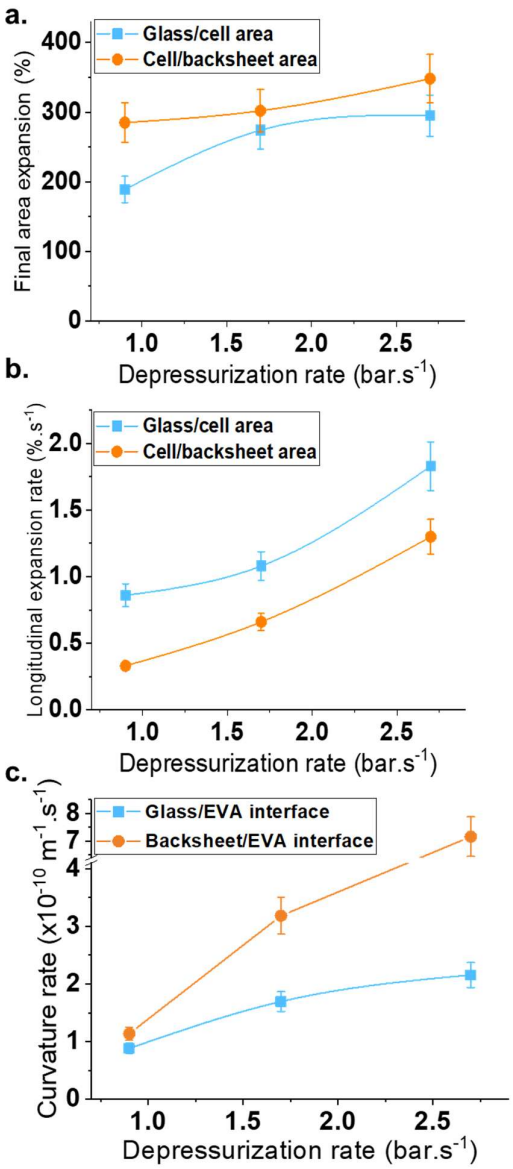

Fig. 13. (a) Final area expansion, **(b)** longitudinal expansion rate, and **(c)** curvature rate of the ethylene-vinyl acetate (EVA) layers in a photovoltaic module as a function of the CO_2 depressurization rate in supercritical CO_2 initially at 150 bar, 75 °C. The lines are drawn to guide the eye.

3.1.2. Effect of the treatment temperature on EVA expansion

While the final area expansion increases linearly with temperature (**Fig. 14a**), the longitudinal expansion rate (**Fig. 14b**) and the curvature rate (**Fig. 14c**) of both EVA layers are slightly lower at 60 °C than at 75 and 90 °C.

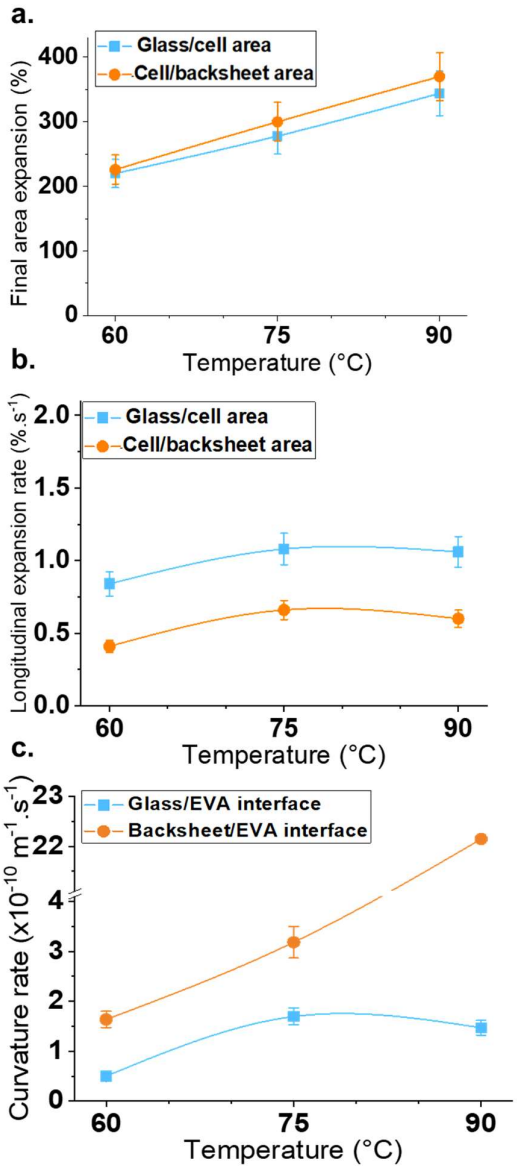

Fig. 14. (a) Final area expansion, **(b)** longitudinal expansion rate, and **(c)** curvature rate of the ethylene-vinyl acetate (EVA) layers in a photovoltaic module as a function of temperature in supercritical CO_2 initially at 150 bar and depressurized at 1.7 bar·s^{-1}. The lines are drawn to guide the eye.

Increasing the temperature reduces the viscosity of polymers [44], which therefore expands more easily [45]. This effect is amplified above the melting temperature, where the viscosity decreases dramatically [44]. For an EVA based polymer, the same effect on rigidity was also measured [46]. As illustrated in **Fig. 15** indeed, while at 60 °C the expansion of the EVA layer is limited by its' semi-crystalline nature, at 90 °C, above the melting point, the polymer is amorphous and the polymer chains far more mobile. This decrease in rigidity explains why the area expansion of the EVA layers increases with temperature and why the longitudinal expansion rate is higher at 75 °C and 90 °C than at 60 °C.

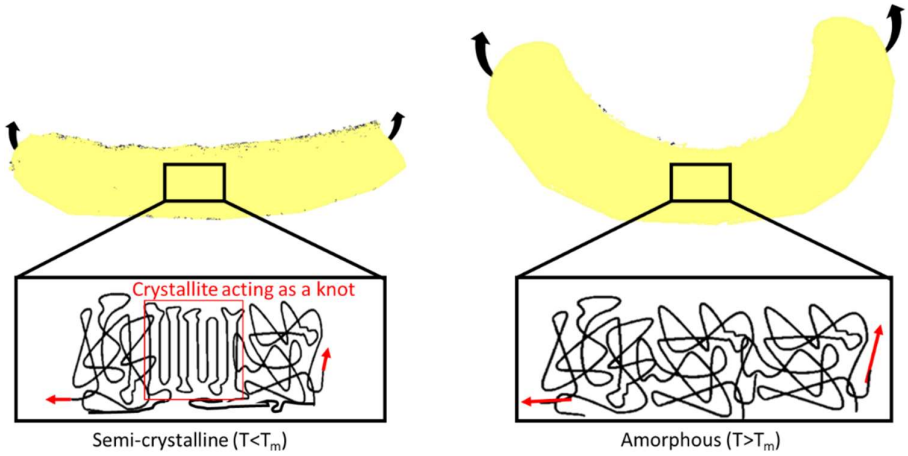

Fig. 15. Schematic illustration of the effect of crystallites on polymer expansion.

3.1.3. Effect of the initial CO_2 pressure on EVA expansion

The results summarized in **Fig. 16** show that there is a threshold CO_2 pressure between 100 and 150 bar below which the EVA layers do not bend at all. Furthermore, while the EVA layer at the backsheet/EVA interface curved more rapidly when the CO_2 was depressurized from 200 rather than 150 bar, the curvature rate at the glass/EVA interface was highest when the initial CO_2 pressure was 150 bar.

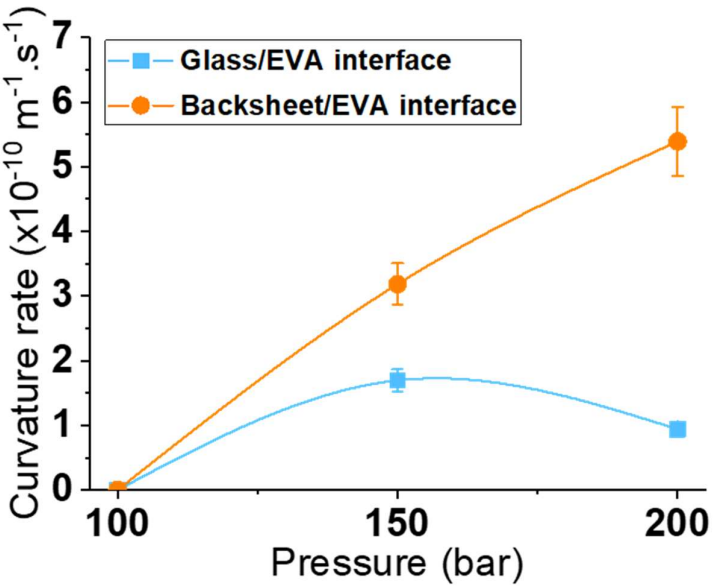

Fig. 16. Curvature rate of the ethylene-vinyl acetate (EVA) layers in a photovoltaic module as a function of the initial pressure in supercritical CO_2 at 150 bar and depressurized at 1.7 bar·s^{-1}. The lines are drawn to guide the eye.

3.2. Loss of adhesion at the glass/EVA interface

At the glass/EVA interface, **Fig. 17a** shows that the loss of adhesion is almost complete (> 90%) at 60 °C and increases further with temperature such that complete delamination is achieved at 90 °C. A similar trend if observed as a function of the depressurization rate in **Fig. 17c**. The results in **Fig. 17b** show that while the loss of adhesion is substantial (~80 %) even at 100 bar, with a low final area expansion of the EVA layer (~ 100 %). At 150 and 200 bar however, the expansion by ~300 % in area of the EVA layer is reflected by almost complete separation, highlighting the major contribution of deformation to the loss of adhesion at this interface. This mechanical effect presumably leads to the tearing of the bonds between the silane groups on the surface of the glass and the EVA.

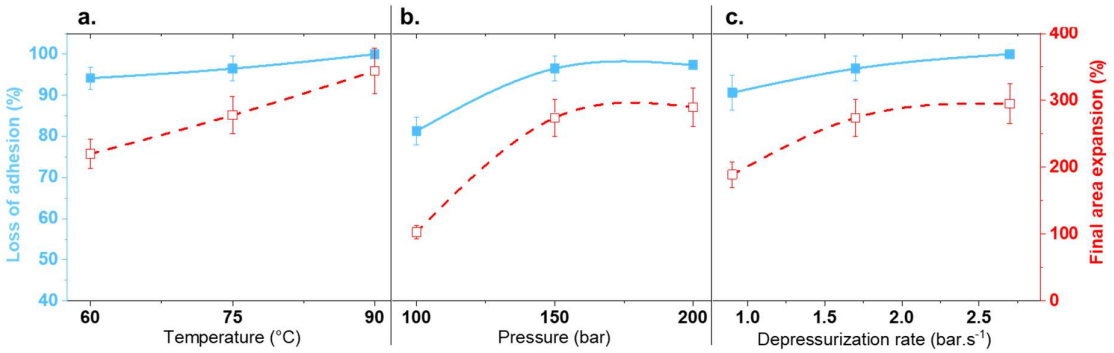

Fig. 17. Loss of adhesion (solid blue squares, left axis) and final area expansion (open red squares, right axis) of the ethyl-vinyl acetate (EVA) layer at the glass/EVA interface in a photovoltaic cell as a function of **(a)** the temperature, **(b)** the initial pressure and **(c)** the depressurization rate of the supercritical CO_2 treatment. The lines are drawn to guide the eye.

3.3. Loss of adhesion at the EVA/backsheet interface

The delamination process at the EVA/backsheet interface is more complex because the backsheet is also sensitive to SC-CO_2, the primer and PVDF layers becoming deformed while the PET core remains rigid. **Fig. 18** highlights the effects of the partial internal separation observed as a result.

Fig. 18. (a) Effect of interface transfer on the peel curve. **(b)** Photograph of a sample with an internally separated backsheet and **(c)** an expanded view of the area inside the black rectangle, showing the separation at the PET/PVDF interface.

At 60 °C, blisters appear on the surface of the primer layer of the backsheet, which is in contact with EVA (**Fig. 19**), inducing complete internal separation at the primer/PET interface. As a result, no peel tests could be performed at 60 °C. **Fig. 20a** shows that the loss of adhesion is greater 75 °C (> 80 %) than at 90 °C (~ 70 %), while the final area expansion increases linearly with temperature. The trends in terms of the pressure and depressurization are very similar, both for the loss of adhesion (**Fig. 20b**) and the final area expansion (**Fig. 20c**), which increase slightly from about 80 to 90% and from about 280 to 320%, respectively, over the ranges considered. The close correlation between the levels of delamination and area expansion indicates that mechanical effects play a major role in the separation of the EVA and backsheet layers, while the results in terms of temperature highlight the potential perturbations that can arise from the backsheet's multilayer structure.

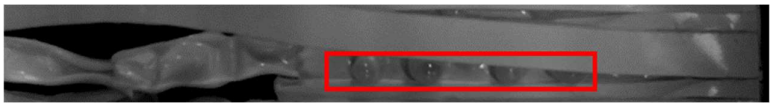

Fig. 19. Photograph of a peel test specimen treated at 60 °C, 150 bar and 1.7 bar·s^{-1} with the red rectangle highlighting blistering at the surface of the primer layer in contact with the foamed ethylene-vinyl acetate.

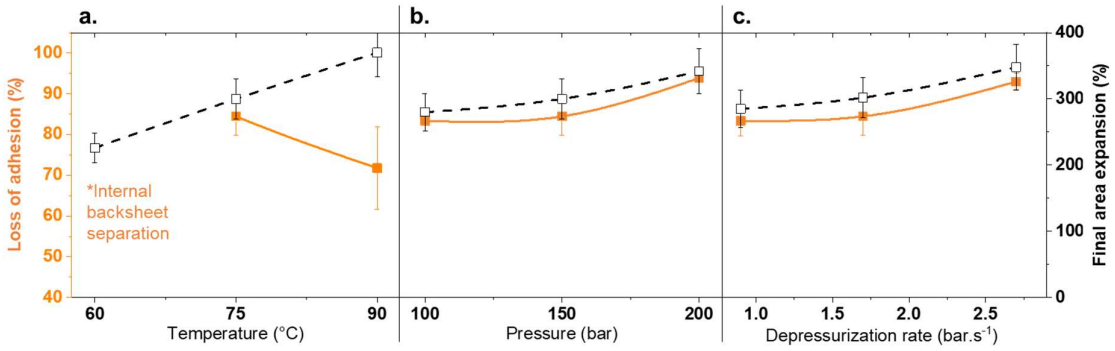

Fig. 20. Loss of adhesion (solid orange squares, left axis) and final area expansion (open black squares, right axis) of the ethyl-vinyl acetate (EVA) layer at the EVA/backsheet interface as a function of **(a)** the temperature, **(b)** the initial pressure and **(c)** the depressurization rate of the

supercritical CO_2 treatment. The lines are drawn to guide the eye. **(a)** At 60 °C, the backsheet layer separated internally rather than at the interface with the EVA layer.

3.4. Loss of adhesion at the cell-frontside/EVA interface

At the front side of the cell, the loss of adhesion increases from a low level (~40 %) at 60 °C to around 70 % at 75 and 90 °C (**Fig. 21a**). At 60 °C, EVA is still crystalline and more rigid (see section 3.1.2) and it seems this rigidity limits the level of separation obtained at this interface.

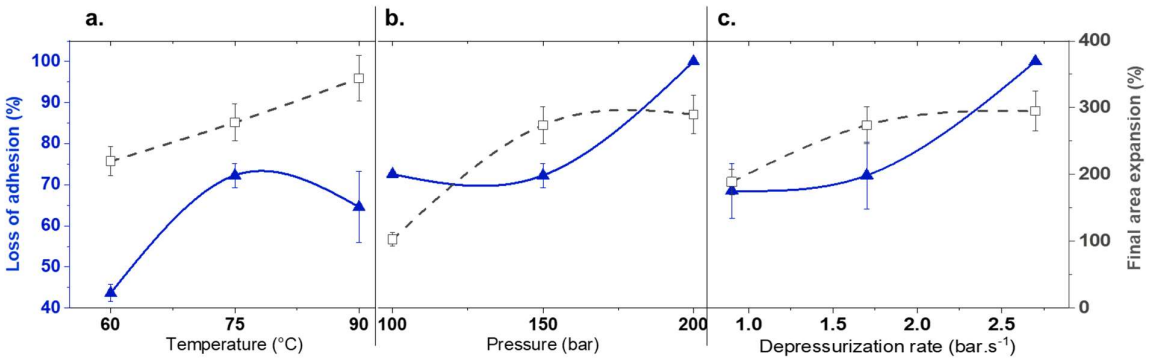

Fig. 21. Loss of adhesion (solid blue triangles, left axis) and final area expansion (open gray squares, right axis) of the ethylene-vinyl acetate (EVA) layer at the cell-frontside/EVA interface as a function of **(a)** the temperature, **(b)** the initial pressure and **(c)** the depressurization rate of the supercritical CO_2 treatment. The lines are drawn to guide the eye.

At 200 bar, the cell-frontside/EVA interface becomes completed delaminated (**Fig. 21b**) because bubbles nucleate in the hollow of the textured front surface of the cell (median nuclei radius (4 µm) [47] ~ acid attack depth (4-5 µm) [38]). When the bubbles grow larger than the distance between two pyramid features, the EVA separates from the cell (**Fig. 22**). The morphology of this interface therefore plays an important role in the delamination process.

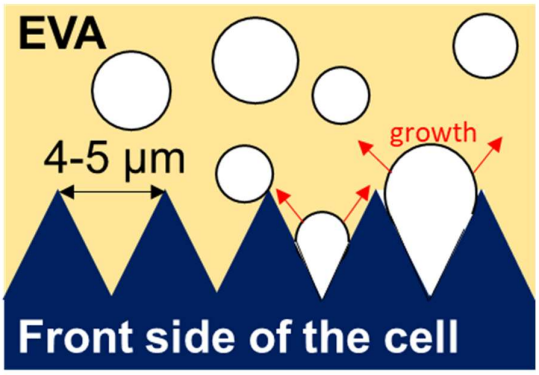

Fig. 22. Schematic representation of the effects of CO_2 bubble formation at the cell-frontside/EVA (ethylene-vinyl acetate) interface during EVA foaming with supercritical CO_2.

Complete separation can also be achieved by increasing the depressurization rate (and thereby the mechanical stress) up to 2.7 bar·s^{-1} (**Fig. 21c**). Note however that the cell samples studied here did not break because they were stiffened with a laminated glass/epoxy structure. In a real PV module, the cell would break and the cell-frontside/EVA interface is therefore unlikely to delaminate completely.

4. Conclusion

This study based on in-situ observations of the deformation of EVA layers in PV modules during SC-CO_2 foaming shows that the expansion of the EVA is enhanced above the melting temperature, that there is a threshold pressure below which the EVA layers do not bend at all, and that the depressurization rate can be increased to maximize all the considered deformation parameters, thereby increasing the mechanical stress at the different interfaces. The level of EVA expansion is shown to be closely correlated with the percentage loss of adhesion induced at the glass/EVA and backsheet/EVA interfaces. The effects of surface texturing at the cell front-side/EVA interface are also highlighted. In summary, this paper shows that EVA foaming with SC-CO_2 has specific effects and leads to different levels of delamination

at the different EVA interfaces in PV modules. This work is of great interest for the identification of suitable operating parameters for the delamination of PV modules using SC-CO_2. Moreover, this process and the approach described in this paper could be applied to the delamination of other types of PV modules or other multilayer structures composed of polymers, such as LCD screens and batteries.

References

[1] I. IRENA, End-Of-Life Management: Solar Photovoltaic Panels, Int. Renew. Energy Agency Int. Energy Agency Photovolt. Power Syst. (2016).

[2] ITRPV, International Technology Roadmap for Photovoltaic (ITRPV) - Results of 2019 - 11th edition, 2020.

[3] Y. Kim, J. Lee, Dissolution of ethylene vinyl acetate in crystalline silicon PV modules using ultrasonic irradiation and organic solvent, Sol. Energy Mater. Sol. Cells. 98 (2012) 317–322. https://doi.org/10.1016/j.solmat.2011.11.022.

[4] X. Xu, D. Lai, G. Wang, Y. Wang, Nondestructive silicon wafer recovery by a novel method of solvothermal swelling coupled with thermal decomposition, Chem. Eng. J. 418 (2021) 129457. https://doi.org/10.1016/j.cej.2021.129457.

[5] V. Savvilotidou, E. Gidarakos, Pre-concentration and recovery of silver and indium from crystalline silicon and copper indium selenide photovoltaic panels, J. Clean. Prod. 250 (2020). https://doi.org/10.1016/j.jclepro.2019.119440.

[6] A. Kuczyńska-Łazewska, E. Klugmann-Radziemska, Influence of fragment size on the time and temperature of ethylene vinyl acetate lamination decomposition in the photovoltaic module recycling process, Materials. 12 (2019). https://doi.org/10.3390/ma12182857.

[7] J. Tao, S. Yu, Review on feasible recycling pathways and technologies of solar photovoltaic modules, Sol. Energy Mater. Sol. Cells. 141 (2015) 108–124. https://doi.org/10.1016/j.solmat.2015.05.005.

[8] C. AYMONIER, Procédé et dispositif de démontage de systèmes multicouches comprenant au moins un composant organique, 2017.

[9] É.S. Lovato, L.M. Donato, P.P. Lopes, E.H. Tanabe, D.A. Bertuol, Application of supercritical CO2for delaminating photovoltaic panels to recover valuable materials, J. CO2 Util. 46 (2021). https://doi.org/10.1016/j.jcou.2021.101477.

[10] A. Briand, A. Leybros, C. Audoin, J.C. Ruiz, F. Lamadie, A. Grandjean, CO2 absorption into a polymer within a multilayer structure: The case of poly(ethylene-co-vinyl acetate) in photovoltaic modules, J. Supercrit. Fluids. 179 (2022) 105380. https://doi.org/10.1016/j.supflu.2021.105380.

[11] J.A. Villamil Jiménez, N. Le Moigne, J.-C. Bénézet, M. Sauceau, R. Sescousse, J. Fages, Foaming of PLA Composites by Supercritical Fluid-Assisted Processes: A Review, Molecules. 25 (2020). https://doi.org/10.3390/molecules25153408.

[12] E. Reverchon, S. Cardea, Production of controlled polymeric foams by supercritical CO2, J. Supercrit. Fluids. 40 (2007) 144–152. https://doi.org/10.1016/j.supflu.2006.04.013.

[13] E. Di Maio, E. Kiran, Foaming of polymers with supercritical fluids and perspectives on the current knowledge gaps and challenges, J. Supercrit. Fluids. (2018).

[14] D. Tammaro, G. D'Avino, E. Di Maio, R. Pasquino, M.M. Villone, D. Gonzales, M. Groombridge, N. Grizzuti, P.L. Maffettone, Validated modeling of bubble growth, impingement and retraction to predict cell-opening in thermoplastic foaming, Chem. Eng. J. 287 (2016) 492–502. https://doi.org/10.1016/j.cej.2015.11.034.

[15] J.L. Sumey, J.A. Sarver, E. Kiran, Foaming of polystyrene and poly(methyl methacrylate) multilayered thin films with supercritical carbon dioxide, J. Supercrit. Fluids. 145 (2019) 243–252. https://doi.org/10.1016/j.supflu.2018.12.001.

[16] S. Sanyal, Q. Ke, Y. Zhang, T. Ngo, J. Carrell, H. Zhang, L.L. Dai, Understanding and optimizing delamination/recycling of printed circuit boards using a supercritical carbon dioxide process, J. Clean. Prod. 41 (2013) 174–178. https://doi.org/10.1016/j.jclepro.2012.10.011.

[17] H.E. Naguib, C.B. Park, N. Reichelt, Fundamental foaming mechanisms governing the volume expansion of extruded polypropylene foams, J. Appl. Polym. Sci. 91 (2004) 2661–2668. https://doi.org/10.1002/app.13448.
[18] J. Wang, P.C. Lee, C.B. Park, Visualization of initial expansion behavior of butane-blown low-density polyethylene foam at extrusion die exit, Polym. Eng. Sci. 51 (2011) 492–499. https://doi.org/10.1002/pen.21803.
[19] H.E. Naguib, C.B. Park, U. Panzer, N. Reichelt, Strategies for achieving ultra low-density polypropylene foams, Polym. Eng. Sci. 42 (2002) 1481–1492. https://doi.org/10.1002/pen.11045.
[20] J.W.S. Lee, K. Wang, C.B. Park, Challenge to Extrusion of Low-Density Microcellular Polycarbonate Foams Using Supercritical Carbon Dioxide, Ind. Eng. Chem. Res. 44 (2005) 92–99. https://doi.org/10.1021/ie0400402.
[21] P.C. Lee, W. Kaewmesri, J. Wang, C.B. Park, J. Pumchusak, R. Folland, A. Praller, Effect of die geometry on foaming behaviors of high-melt-strength polypropylene with CO2, J. Appl. Polym. Sci. 109 (2008) 3122–3132. https://doi.org/10.1002/app.28204.
[22] K. Taki, K. Tabata, S. Kihara, M. Ohshima, Bubble coalescence in foaming process of polymers, Polym. Eng. Sci. 46 (2006) 680–690. https://doi.org/10.1002/pen.20521.
[23] J.A. Sarver, J.L. Sumey, M.L. Williams, J.P. Bishop, D.M. Dean, E. Kiran, Foaming of poly(ethylene-co-vinyl acetate) and poly(ethylene-co-vinyl acetate-co-carbon monoxide) and their blends with carbon dioxide, J. Appl. Polym. Sci. 135 (2018) 45841. https://doi.org/10.1002/app.45841.
[24] S. Siripurapu, J.A. Coughlan, R.J. Spontak, S.A. Khan, Surface-constrained foaming of polymer thin films with supercritical carbon dioxide, Macromolecules. 37 (2004) 9872–9879. https://doi.org/10.1021/ma0484983.
[25] J. Li, X. Liao, Q. Jiang, W. Wang, G. Li, Creating orientated cellular structure in thermoplastic polyurethane through strong interfacial shear interaction and supercritical carbon dioxide foaming for largely improving the foam compression performance, J. Supercrit. Fluids. 153 (2019). https://doi.org/10.1016/j.supflu.2019.104577.
[26] F.M. Fowkes, ATTRACTIVE FORCES AT INTERFACES, Ind. Eng. Chem. 56 (1964) 40–52. https://doi.org/10.1021/ie50660a008.
[27] J. Padday, Handbook of adhesion, Wetting Word Adhes. (1992) 594.
[28] D.K. Owens, R.C. Wendt, Estimation of the surface free energy of polymers, J. Appl. Polym. Sci. 13 (1969) 1741–1747. https://doi.org/10.1002/app.1969.070130815.
[29] S. Wu, Polar and nonpolar interactions in adhesion, J. Adhes. 5 (1973) 39–55. https://doi.org/10.1080/00218467308078437.
[30] A.N. Gent, S.-M. Lai, Adhesion and Autohesion of Rubber Compounds: Effect of Surface Roughness, Rubber Chem. Technol. 68 (1995) 13–25. https://doi.org/10.5254/1.3538725.
[31] J.W. McBain, D.G. Hopkins, On Adhesives and Adhesive Action, J. Phys. Chem. 29 (1925) 188–204. https://doi.org/10.1021/j150248a008.
[32] D.E. Packham, Surface energy, surface topography and adhesion, Int. J. Adhes. Adhes. 23 (2003) 437–448. https://doi.org/10.1016/S0143-7496(03)00068-X.
[33] S.S. Voyutskii, V.L. Vakula, The role of diffusion phenomena in polymer-to-polymer adhesion, J. Appl. Polym. Sci. 7 (1963) 475–491. https://doi.org/10.1002/app.1963.070070207.
[34] R.P. Wool, Polymer interfaces: structure and strength, Hanser Publishers, 1995.
[35] J. Tracy, N. Bosco, R. Dauskardt, Encapsulant Adhesion to Surface Metallization on Photovoltaic Cells, IEEE J. Photovolt. 7 (2017) 1635–1639. https://doi.org/10.1109/JPHOTOV.2017.2746572.
[36] V. Chapuis, V. Pélisset, M. Raeis-Barnéoud, H.-Y. Li, L.-E. Perret-Aebi, Compressive-shear adhesion characterization of polyvinyl-butyral and ethylene-vinyl acetate at

different curing times before and after exposure to damp-heat conditions, Prog. Photovolt. Res. Appl. 22 (2014) 405–414. https://doi.org/10.1002/pip.2270.
[37] S.R. Leadley, J. Watts, The use of XPS to examine the interaction of poly(acrylic acid) with oxidised metal substrates, J. Electron Spectrosc. Relat. Phenom. 85 (1997) 107–121. https://doi.org/10.1016/S0368-2048(97)00028-5.
[38] R. Einhaus, E. Vazsonyi, J. Szlufcik, J. Nijs, R. Mertens, Isotropic texturing of multicrystalline silicon wafers with acidic texturing solutions, Twenty Sixth IEEE Photovolt. Spec. Conf. (1997).
[39] B.R.K. Blackman, Fracture Tests, in: L.F.M. da Silva, A. Öchsner, R.D. Adams (Eds.), Handb. Adhes. Technol., Springer Berlin Heidelberg, Berlin, Heidelberg, 2011: pp. 473–501. https://doi.org/10.1007/978-3-642-01169-6_20.
[40] AFNOR, Adhésifs - Essai de pelage pour un assemblage collé flexible-sur-rigide - Partie 2 : pelage à 180 degrés, (2011).
[41] G.J. Jorgensen, K.M. Terwilliger, J.A. DelCueto, S.H. Glick, M.D. Kempe, J.W. Pankow, F.J. Pern, T.J. McMahon, Moisture transport, adhesion, and corrosion protection of PV module packaging materials, Sol. Energy Mater. Sol. Cells. 90 (2006) 2739–2775. https://doi.org/10.1016/j.solmat.2006.04.003.
[42] B. Adothu, P. Bhatt, S. Chattopadhyay, S. Zele, J. Oderkerk, H. Sagar, F. Costa, S. Mallick, Newly developed thermoplastic polyolefin encapsulant-A potential candidate for crystalline silicon photovoltaic modules encapsulation, Sol. ENERGY. 194 (2019) 581–588. https://doi.org/10.1016/j.solener.2019.11.018.
[43] N. Theut, A. Jeffries, R. Kumar, G. von Gastrow, D. Fenning, M. Bertoni, IEEE, The Influence of Water Content on the Adhesion Between Solar Module Interfaces, in: 2020: pp. 2057–2061.
[44] S. Curia, D.S.A. De Focatiis, S.M. Howdle, High-pressure rheological analysis of CO2-induced melting point depression and viscosity reduction of poly(ε-caprolactone), Self-Heal. Polym. 69 (2015) 17–24. https://doi.org/10.1016/j.polymer.2015.05.026.
[45] R. Liao, W. Yu, C. Zhou, Rheological control in foaming polymeric materials: I. Amorphous polymers, Polymer. 51 (2010) 568–580. https://doi.org/10.1016/j.polymer.2009.11.063.
[46] J.A. Sarver, J.C. Hassler, E. Kiran, Linking thermophysical and rheological properties to the selection of CO2 foaming conditions of rubbery elastomers using the relative rigidity reduction path, J. Supercrit. Fluids. 166 (2020). https://doi.org/10.1016/j.supflu.2020.105015.
[47] A. Briand, A. Leybros, O. Doucet, J.C. Ruiz, F. Lamadie, A. Grandjean, A microscopic study of bubble nucleation and growth in ethylene-vinyl acetate foaming by supercritical CO2, ("Unpublished results").